

# SCIENTIFIC REPORTS



OPEN

## Synthesis of Fe<sub>16</sub>N<sub>2</sub> compound Free-Standing Foils with 20 MGOe Magnetic Energy Product by Nitrogen Ion-Implantation

Yanfeng Jiang<sup>1</sup>, Md Al Mehedi<sup>2</sup>, Engang Fu<sup>3</sup>, Yongqiang Wang<sup>3</sup>, Lawrence F. Allard<sup>4</sup> & Jian-Ping Wang<sup>1,2</sup>

Received: 06 November 2015

Accepted: 12 April 2016

Published: 05 May 2016

Rare-earth-free magnets are highly demanded by clean and renewable energy industries because of the supply constraints and environmental issues. A promising permanent magnet should possess high remanent magnetic flux density ( $B_r$ ), large coercivity ( $H_c$ ) and hence large maximum magnetic energy product ( $(BH)_{max}$ ). Fe<sub>16</sub>N<sub>2</sub> has been emerging as one of promising candidates because of the redundancy of Fe and N on the earth, its large magnetocrystalline anisotropy ( $K_u > 1.0 \times 10^7$  erg/cc), and large saturation magnetization ( $4\pi M_s > 2.4$  T). However, there is no report on the formation of Fe<sub>16</sub>N<sub>2</sub> magnet with high  $B_r$  and large  $H_c$  in bulk format before. In this paper, we successfully synthesize free-standing Fe<sub>16</sub>N<sub>2</sub> foils with a coercivity of up to 1910 Oe and a magnetic energy product of up to 20 MGOe at room temperature. Nitrogen ion implantation is used as an alternative nitriding approach with the benefit of tunable implantation energy and fluence. An integrated synthesis technique is developed, including a direct foil-substrate bonding step, an ion implantation step and a two-step post-annealing process. With the tunable capability of the ion implantation fluence and energy, a microstructure with grain size 25–30 nm is constructed on the FeN foil sample with the implantation fluence of  $5 \times 10^{17}/\text{cm}^2$ .

Rare-earth-free magnets are highly demanded by clean and renewable energy industries because of the supply constraints and environmental issues of rare-earth permanent magnets in recent years<sup>1</sup>. Among many candidates being pursued<sup>1,2</sup>, Fe<sub>16</sub>N<sub>2</sub> has been emerging as one of promising candidates because of the redundancy of Fe and N on the earth, its large magnetocrystalline anisotropy ( $K_u > 1.0 \times 10^7$  erg/cc), and large saturation magnetization ( $4\pi M_s > 2.4$  T)<sup>3</sup>. A promising permanent magnet should have high  $M_s$ , large coercivity ( $H_c$ ) and hence, large energy product. In this sense,  $\alpha''$ -Fe<sub>16</sub>N<sub>2</sub> could be a promising permanent magnet<sup>3,4</sup>. Its theoretical energy product is estimated as high as 135 MGOe, corresponding to a fully packed single domain microstructure<sup>3</sup>. Many research groups have investigated  $\alpha''$ -Fe<sub>16</sub>N<sub>2</sub> during the last 40 years<sup>2,3,5–10</sup>, while attempting many preparation methods. However, there is no report on the formation of Fe<sub>16</sub>N<sub>2</sub> magnet with high  $B_r$  and large  $H_c$  in bulk format yet. Based on previous experience in  $\alpha''$ -Fe<sub>16</sub>N<sub>2</sub> thin film preparation, suitable nitrogen concentration (11.1 at.%) is necessary for a high volume ratio of  $\alpha''$ -Fe<sub>16</sub>N<sub>2</sub> phase<sup>3,11</sup>. At the same time, residual strain is also one of the key aspects needed to induce martensite phase formation and achieve giant  $M_s$ <sup>12</sup>. Moreover, its microstructure, including grain size and grain boundary, should be optimized at the same time to achieve high coercivity<sup>13</sup>. So, nitriding, strain and microstructure are the three important aspects of Fe<sub>16</sub>N<sub>2</sub> permanent magnet preparation.

So far, no approach is reported to prepare Fe<sub>16</sub>N<sub>2</sub> bulk samples, which could optimize all these three key aspects, including nitriding, strain and microstructure, at the same time. We suspect that some contradictions are aroused by the discrepancy between inherent material properties and required technical parameters. For example, the microstructure of a permanent magnet can be adjusted during the post-annealing process by changing the annealing temperature<sup>13</sup>. For Fe-based material, its microstructure can be tuned when the annealing temperature above 300 °C<sup>14</sup>. However,  $\alpha''$ -Fe<sub>16</sub>N<sub>2</sub> is a martensite phase and can only be stable under 214 °C<sup>2</sup>. This

<sup>1</sup>Department of Electrical and Computer Engineering, University of Minnesota, Minneapolis, MN 55455 USA.

<sup>2</sup>Department of Chemical Engineering and Materials Science, University of Minnesota, Minneapolis, MN 55455 USA.

<sup>3</sup>Ion Beam Material Laboratory, Los Alamos National Laboratory, Los Alamos, New Mexico 87545 USA. <sup>4</sup>Materials Science and Technology Division, Oak Ridge National Laboratory, Tennessee 37831, USA. Correspondence and requests for materials should be addressed to J.-P.W. (email: jpwang@umn.edu)

	Nitride	Strain	Microstructure	Magnetic property
Thin film	Plasma nitriding during deposition	Strain by lattice mismatch between FeN layer and substrate (Giant Ms)	No action (Low coercivity)	soft magnetic property
Powder	Nitriding in wide range temperatures (150 °C to 650 °C)	No strain (No giant Ms)	No action (Coercivity depends on its size)	Soft magnetic property on larger particles, hard magnetic property on small particle (<50 nm)

**Table 1. Technical status of, and main obstructions to, permanent magnet preparation using thin film or powder<sup>3,4,8–10,12,22</sup>.**

contradiction means the microstructure of  $\alpha''$ -Fe<sub>16</sub>N<sub>2</sub> can't be directly tuned by traditional annealing method. This is why, until now, there isn't any report on how to tune the microstructure on  $\alpha''$ -Fe<sub>16</sub>N<sub>2</sub> bulk sample yet.

Table 1 shows the current technical status on these three aspects<sup>2,3</sup>. For thin film samples, the lattice mismatch acting as a strain source plays an important role in the phase transformation<sup>3,4,15</sup> and giant Ms could be observed on thin film samples. While for powder samples, no strain is applied and the corresponding Ms is always lower than Fe<sup>8–10</sup>. No result has been published on how to construct a suitable microstructure in  $\alpha''$ -Fe<sub>16</sub>N<sub>2</sub> thin film and powder. So, for the thin film sample and the powder sample with large particle size (>50 nm), partial soft magnetic property is always observed. While the powder samples with smaller particle size (<50 nm), were reported to exhibit higher coercivity<sup>8–10</sup> because the particle size is coincidental in the range of required grain size for high coercivity<sup>13</sup>.

To prepare an  $\alpha''$ -Fe<sub>16</sub>N<sub>2</sub> permanent magnet in bulk format, it is strategically important to investigate one synthesis technique, by which nitriding, strain and microstructure engineering could be all taken into consideration.

Here we use a nitrogen implantation technique to prepare bulk  $\alpha''$ -Fe<sub>16</sub>N<sub>2</sub> with hard magnetic property. Nitrogen ion implantation is considered as an alternative nitriding approach with the benefit of tunable implantation energy and fluence. Ion-implantation methods can be considered as an approach to prepare bulk  $\alpha''$ -Fe<sub>16</sub>N<sub>2</sub> samples since it is a commercially established technology in the semiconductor industry. By this method, the nitrogen concentration and penetrable depth can be controlled precisely. This technique was used by other groups to prepare Fe<sub>16</sub>N<sub>2</sub> thin film<sup>6,7,16,17</sup> and its feasibility was demonstrated by tuning the implantation energy and fluence. However, there wasn't any reported coercivity on the implanted samples. Furthermore, it was found that the  $\alpha''$ -Fe<sub>16</sub>N<sub>2</sub> phase disappeared when the thickness was over 230 nm<sup>18</sup>, possibly caused by the fact that the  $\alpha''$ -Fe<sub>16</sub>N<sub>2</sub> phase was unstable under high ion fluence and transformed into  $\epsilon$  nitride phase. These problems hindered the application of this technique on bulk  $\alpha''$ -Fe<sub>16</sub>N<sub>2</sub> preparation.

The main technical strategy involves nitrogen implantation into free-standing iron foils and transformation into Fe<sub>16</sub>N<sub>2</sub> phase assisted by the thermal strain during the annealing process. By tuning the fluence, a suitable microstructure can be obtained<sup>19</sup>, corresponding to high coercivity, and hence hard magnetic property.

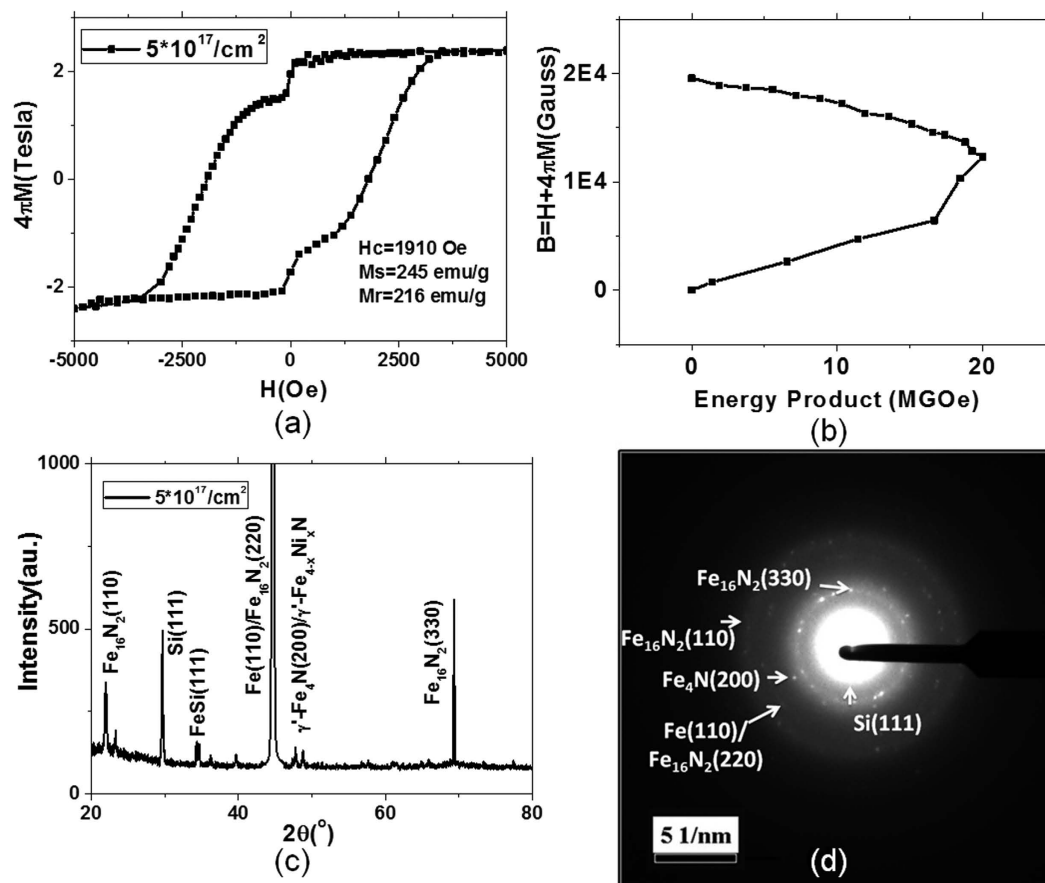
Nakajima *et al.* for first time used the nitrogen ion implantation process to prepare Fe<sub>16</sub>N<sub>2</sub> thin film deposited on a substrate<sup>7,20</sup>, but the Fe<sub>16</sub>N<sub>2</sub> layer is neither free-standing material nor possessing any hard magnetic property, e.g. very low coercivity. In this paper, we successfully synthesize free-standing Fe<sub>16</sub>N<sub>2</sub> foils with a coercivity of up to 1910 Oe and a magnetic energy product of up to 20 MGoe at room temperature. An integrated synthesis technique is developed, including a direct foil-substrate bonding step, an ion implantation step and a two-step post-annealing process. With the tunable capability of the ion implantation fluence and energy, a microstructure with grain size 25–30 nm is constructed in the FeN foil sample with the implantation fluence of  $5 \times 10^{17}/\text{cm}^2$ .

Figure 1 shows the relevant characterization results of a sample with  $5 \times 10^{17}/\text{cm}^2$  fluence. A hard magnetic property with high coercivity (1910 Oe), high Ms (245 emu/g), and promising energy product (Max. 20 MGoe) is clearly observed on the sample. Figure 1(a) shows in-plane hysteresis loops for the sample at room temperature. There is an obvious shoulder at low field, indicating two different magnetic phases existing in the sample and coupling through the exchange-spring effect<sup>21</sup>. The direct calculated energy product is shown in Fig. 1(b), showing its maximum value to be 20 MGoe. The X-ray diffraction spectrum of the sample, as shown in Fig. 1(c), indicates a partial Fe<sub>16</sub>N<sub>2</sub> phase coexisting with Fe and Fe<sub>4</sub>N phases. The crystalline structure is demonstrated by the transmission electron microscopy (TEM) diffraction pattern, as shown in Fig. 1(d).

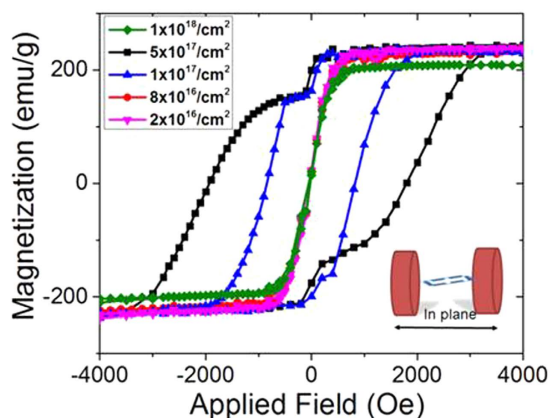
## Results

Figure 2 shows room temperature M-H loops for the sample with different fluence at 100 keV implantation energy. The characterization is conducted in the foil plane using a Vibrating Sample Magnetometer (VSM) calibrated by a standard Ni sample at room temperature. Compared to 206 emu/g for the control sample (the starting single crystal iron foil), four samples, with fluences of  $2 \times 10^{16}/\text{cm}^2$ ,  $8 \times 10^{16}/\text{cm}^2$ ,  $1 \times 10^{17}/\text{cm}^2$  and  $5 \times 10^{17}/\text{cm}^2$ , exhibit high Ms, varying from 230 emu/g to 245 emu/g with different volume ratio of Fe<sub>16</sub>N<sub>2</sub> phase. For the sample with  $1 \times 10^{18}/\text{cm}^2$  fluence, its Ms value drops to 208 emu/g because of the absence of Fe<sub>16</sub>N<sub>2</sub> phase with high fluence.

To get a clear picture on the influence of the formed Fe<sub>16</sub>N<sub>2</sub> phase on magnetic properties of the samples, Figure S5 in supplementary section shows the hysteresis loops before ion implantation and before post-annealing. As shown in Fig. S5, for the pure iron foil before ion-implantation, its magnetic property is in good agreement with Fe (110) single crystal (loop a). Its remanent magnetization value is equal to its saturation magnetization value, which is around 206 emu/g at room temperature. For the sample after the ion-implantation and 500 °C  $\times$  0.5 hr pre-annealing step (loop b), its saturation magnetization increases about 7%, up to 221 emu/g. Meanwhile, its



**Figure 1.** Characterization results of a bulk  $\text{Fe}_{16}\text{N}_2$  free-standing foil prepared by the nitrogen ion implantation method with  $5 \times 10^{17}/\text{cm}^2$  fluence (a) In-plane hysteresis loops for the sample at room temperature, showing  $H_c = 1910$  Oe,  $M_s = 245$  emu/g,  $M_r = 216$  emu/g; (b) The calculated energy product, indicating maximum value 20 MGOe; (c) The X-ray diffraction spectrum, showing the  $\text{Fe}_{16}\text{N}_2$  phase generated in the foil; (d) The HRTEM diffraction pattern of FeN sample with  $5 \times 10^{17}/\text{cm}^2$  fluence, showing  $\text{Fe}_{16}\text{N}_2$ ,  $\text{Fe}_4\text{N}/\text{Fe}_{4-x}\text{Ni}_x\text{N}$  and Fe phases.



**Figure 2.** In-plane hysteresis loops for the samples with different fluences at room temperature. Samples with  $2 \times 10^{16}/\text{cm}^2$ ,  $8 \times 10^{16}/\text{cm}^2$  and  $1 \times 10^{18}/\text{cm}^2$  fluences show soft magnetic property, while samples with  $1 \times 10^{17}/\text{cm}^2$  and  $5 \times 10^{17}/\text{cm}^2$  exhibit hard magnetic property.

remanent magnetization value is reduced and its saturation field ( $H_s$ ) is enhanced up to about 1000 Oe, which indicates the existence of the  $\text{Fe}_8\text{N}$  phase after the pre-annealing step.

The successive post-annealing step at 150 °C for 40 hrs tremendously changes the M-H loop of the sample, which matches well with the formation of the  $\text{Fe}_{16}\text{N}_2$  phase in the sample as indicated in Fig. 2. As shown by

hysteresis loops in Fig. 2, a hard magnetic behavior is clearly observed with its saturation field up to 3.8 kOe. This is consistent with the existence of large magnetocrystalline anisotropy due to the body-center-tetragonal (bct) structure in  $\text{Fe}_{16}\text{N}_2$ <sup>3,22,23</sup>. More importantly, a 15% increase in the saturation magnetization is observed in this sample, which is much beyond the VSM testing error. The absolute  $M_s$  value is up to 245 emu/g under  $5 \times 10^{17}/\text{cm}^2$  fluence, compared to 206 emu/g for the control sample (the starting single crystal iron foil). XRD patterns as shown in Fig. S3 and TEM analysis shown in Fig. S4 present clearly the mixed phases of Fe and  $\text{Fe}_{16}\text{N}_2$  in the sample. Based on an XPS method<sup>24</sup>, the estimated volume ratio for the  $\text{Fe}_{16}\text{N}_2$  phase in this sample under  $5 \times 10^{17}/\text{cm}^2$  fluence is about 35%. Thus, the saturation magnetization of  $\text{Fe}_{16}\text{N}_2$  phase in this sample is calculated as about 296 emu/g (2.9 T). For this calculation, we assume that the Fe matrix in the sample possesses the same saturation magnetization before the ion-implantation and annealing, which is reasonable, since we used the same sample before and after ion-implantation. This giant saturation magnetization is consistent with the proposed theory<sup>15</sup> and recent report on thin film samples<sup>3,12</sup>. For sample with fluence  $1 \times 10^{18}/\text{cm}^2$ , the  $\text{Fe}_{16}\text{N}_2$  phase decreases while the  $\gamma'$ - $\text{Fe}_4\text{N}/\text{Fe}_{4-x}\text{Ni}_x\text{N}$  phase increases, showing that  $\text{Fe}_{16}\text{N}_2$  is unstable at higher fluence and decomposes into  $\gamma'$ - $\text{Fe}_4\text{N}/\text{Fe}_{4-x}\text{Ni}_x\text{N}$  phase.

As shown in Fig. 1(c), FeSi (111) phase is generated. This indicates that Fe foil may be mixed with silicon substrate top surface during the sample preparation because of a lower surface energy of Si compared to that of Fe. Surface energy is one of the most fundamental parameters of a solid since it depends directly on the binding forces of the material. Indeed, it is a measure of the work necessary to separate a material into two parts along a plane. The surface energy of Si (111)<sup>25</sup> is 1230 ergs/cm<sup>2</sup> while the surface energy of Fe (110)<sup>26</sup> is 2500 ergs/cm<sup>2</sup>. During the bonding process at 450 °C, silicon atoms could be cleaved and diffuse into Fe foil.

It is possible to produce  $\text{Fe}_{4-x}\text{Ni}_x\text{N}$  during annealing accompanied with the generation of  $\text{Fe}_4\text{N}$ , in which Ni atoms occupy the FCC positions ( $\text{Fe}^f$ ) of the  $\text{Fe}_4\text{N}$  in a random manner<sup>27</sup>. While the Ni atoms in  $\text{Fe}_{4-x}\text{Ni}_x\text{N}$  lattice carry zero magnetic moment, the magnetic moment in  $\text{Fe}_{4-x}\text{Ni}_x\text{N}$  is decreased accordingly. While high  $M_s$  value is observed in the implanted sample, it means that the volume ratio of  $\text{Fe}_{4-x}\text{Ni}_x\text{N}$  is not high enough to cancel the contribution of  $\alpha''$ - $\text{Fe}_{16}\text{N}_2$  phase. For the sample with fluence  $5 \times 10^{17}/\text{cm}^2$ , only 1% to 2% of  $\text{Fe}_4\text{N} + \text{Fe}_{4-x}\text{Ni}_x\text{N}$  exists in the sample. The influence of magnetic moment degradation of  $\text{Fe}_{4-x}\text{Ni}_x\text{N}$  can be neglected. But for the sample with fluence  $1 \times 10^{18}/\text{cm}^2$ , volume ratio of  $\text{Fe}_4\text{N} + \text{Fe}_{4-x}\text{Ni}_x\text{N}$  increases to 5% to 6%. The reason for the degradation of the  $M_s$  value of the sample should come from two aspects: decrement of the  $\alpha''$ - $\text{Fe}_{16}\text{N}_2$  phase and increment of  $\text{Fe}_{4-x}\text{Ni}_x\text{N}$  phase. To obtain sample with high  $M_s$  value,  $\text{Fe}_{4-x}\text{Ni}_x\text{N}$  phase should be avoided in future experiment.

For samples with fluences of  $1 \times 10^{17}/\text{cm}^2$  and  $5 \times 10^{17}/\text{cm}^2$ , obvious flatness in the hysteresis loops can be observed, as shown in Fig. 2, identical to the behavior demonstrated for the exchange-spring magnets<sup>21</sup>. Another obvious evidence for the exchange coupling is that the ratio  $M_r/M_s$  in the well-processed samples is greater than 0.8<sup>28</sup>.

## Discussion

We experimentally demonstrate an integrated synthesis method to prepare  $\alpha''$ - $\text{Fe}_{16}\text{N}_2$  permanent magnets based on free-standing Fe foil samples with a thickness of 500 nm. The three key aspects for  $\alpha''$ - $\text{Fe}_{16}\text{N}_2$  permanent magnet preparation, including nitriding, strain and microstructure engineering, are addressed simultaneously in this method.

Nitrogen is introduced directly by the implantation method. For our experiment, the beam current density is  $4 \mu\text{A}/\text{cm}^2$ . The target temperature was intended at room temperature. The beam heating causes some temperature rise but usually no more than 50 °C since the active cooling on the sample stage was used. Generally the heat generated by high energy ion implantation would release the nitrogen atoms and also cause the phase transformation. The usage of high energy ion implantation above 100 keV was not possible to obtain  $\text{Fe}_{16}\text{N}_2$ <sup>17</sup>. Ion beam voltage has to be below 100 keV and current should be low to keep foil at low temperature. It was demonstrated experimentally that N<sup>+</sup> ion implantation with ion beam voltage of no more than 100 keV and current less than  $5 \mu\text{A}$  was effective for  $\text{Fe}_{16}\text{N}_2$  formation<sup>17,29</sup>. On the other side, low implantation energy (less than 100 keV) is also not good for  $\alpha''$ - $\text{Fe}_{16}\text{N}_2$  phase formation because of the requirement from the enthalpy of formation of  $\alpha''$ - $\text{Fe}_{16}\text{N}_2$ <sup>28</sup>. The implantation energy determines the penetration depth directly. To get homogeneous distribution of nitrogen inside sample, a long term post-annealing is always required. If implantation energy is less than 100 keV, the post-annealing time will be prolonged correspondingly. A tradeoff between a reasonable annealing time and a good penetration depth should be considered. In this sense, the best implantation condition in this study is 100 keV.

To prevent nitrogen from escaping during annealing, a nickel layer was deposited on the surface of the foil<sup>30</sup>. Nickel cover layer is helpful in keeping nitrogen atoms inside. This is also helpful for nitrogen homogeneous distribution. To clean the absorbed oxygen on the iron surface, a surface reduction step was conducted before nickel deposition with 10%  $\text{H}_2 + 90\% \text{N}_2$  at 200 °C for 10 mins.

For the implanted nitrogen atoms, they are inert and deactivated before activation treatment. The pre-annealing step acts as an activation process to activate the implanted nitrogen. Temperature was increased to 500 °C to initiate the activation and remained at 500 °C for 0.5 hr to assist the activation over the entire wafer. Besides the function for activation, the pre-annealing step also helped to repair the lattice damage at 500 °C in Ar.

The strain is generated during the post-annealing process because of the mismatch of thermal coefficients between Fe foil and Fe substrate. Figure S6 in supporting material shows the strain by comparing XRD spectrum before and after annealing.

As for the microstructure, implanted ions with suitable fluence and energy can lead to specific grain size in the sample<sup>19</sup>.

Before post-annealing, nitrogen atoms are arranged in a disordered manner. The phase transformation into  $\alpha'$  corresponds to a rearrangement of nitrogen atoms, resulting in an ordered pattern. Therefore, the post-annealing step assists with the ordering of the nitrogen atoms.

The other benefit of the long annealing time is the mechanical equilibrium of strain in foil. The thermal expansion coefficients of the iron foil and silicon substrate are  $11.8 \mu\text{m/m}\cdot\text{K}$  and  $2.6 \mu\text{m/m}\cdot\text{K}$ , respectively. The difference in the coefficients of linear thermal expansion between the iron and silicon will lead to the compressive stress on the iron foil. This difference  $\Delta\alpha(T)$  is nearly constant between room temperature (RT) and the annealing temperature  $150^\circ\text{C}$ . If the annealing is in mechanical equilibrium, that is, if the tension strain is commensurate with the Si substrate, a compressive strain will develop in the foil<sup>31</sup>:

$$\frac{1}{1 - \varepsilon} = \exp\left[\int_{\text{RT}}^{T_A} dT\Delta\alpha(T)\right] \quad (1)$$

where  $\varepsilon$  denotes the strain and  $T_A$  is the annealing temperature.

The calculated linear compressive strain at  $150^\circ\text{C}$  annealing is about 0.2%. A long annealing time is needed to produce strained foil in mechanical equilibrium.

In this way, a stretching force is generated along  $\langle 001 \rangle$  crystalline direction in the foil with (110) face, which is responsible for the phase transformation from bcc to bct<sup>3</sup>. XRD spectrum in Fig. S2 shows that  $\text{Fe}_{16}\text{N}_2$  phase appeared after the annealing process, which confirms the influence of the stress on the  $\text{Fe}_{16}\text{N}_2$  phase formation.

The third aspect necessary for  $\text{Fe}_{16}\text{N}_2$  permanent magnet is the microstructure engineering, which is directly related with the coercivity. Here it is found that microstructure is influenced by implantation dose at fixed implantation energy.

The coercivity is related to its microstructural profile, as shown in Fig. 3. The TEM sample is obtained by cutting and polishing the foil perpendicular to the surface using a Focused Ion Beam (FIB). It can be seen that there exists an obvious difference in the microstructure. For the four samples, all processes are the same except for variations in the fluences. It can therefore be deduced that the different implanted fluencies are the main reason for the development of a microstructure, and hence the coercivity variations.

Generally, a granular structure, instead of a homogeneous one, is formed on these samples, as shown in Fig. 3. At low fluences ( $2 \times 10^{16}/\text{cm}^2$  and  $8 \times 10^{16}/\text{cm}^2$ ), the microstructure is a clear surface embedded by multiple black dots with diameters around 20 nm, while the distance from each other is 140 nm to 200 nm. The corresponding FFT diffraction shows the black dots are mixture phase of  $\text{Fe}_{16}\text{N}_2$  phase and Fe. For medium fluences ( $1 \times 10^{17}/\text{cm}^2$  and  $5 \times 10^{17}/\text{cm}^2$ ), continuous grains have been generated. For the  $5 \times 10^{17}/\text{cm}^2$  sample (Fig. 3(d)), a much more obvious boundary can be observed.

The granular structure formation can be explained using the stochastic model<sup>19</sup>, accounting for the fluence dependence of the grain size. In this model, three mechanisms were presumed to account for the final grain size: statistical variations of area coverage by the implanted ions, ion channeling, and spontaneous nucleation<sup>19</sup>. The ions do not uniformly cover the surface. They strike the target surface at random points. So, for samples with low fluences, such as  $2 \times 10^{16}/\text{cm}^2$  and  $8 \times 10^{16}/\text{cm}^2$ , some areas will appear nitrogen rich, as shown in Fig. 3(a,b). While at higher fluences, a more homogeneous distribution of implanted nitrogen appears, as shown in Fig. 3(c,d).

In case of medium mass ions of energy in the 100 keV range, the typical defects formed are void-like vacancy clusters composed of few vacancies<sup>18</sup>. For the situation of nitrogen implantation in this paper, such clusters act as traps for impurity atoms at low implantation doses and are progressively transformed into precipitates of new phases when the concentration of the impurity atoms becomes sufficiently high. The presence of these traps is crucial for nitride formation. During post-annealing, the short-range migration of nitrogen atoms toward the impurity atoms precipitates new phases and, consequently, the initially uniform distribution of implanted atoms transforms into a "granular" structure of impurity-rich precipitates embedded in an impurity-poor matrix. This can also be demonstrated by the hysteresis loop shown in Fig. 2. There is an obvious shoulder in the loop, showing two magnetic phases with different coercivity and Ms.

Based on the stochastic model, we have developed a numerical relationship to account for the variation of grain size with the implanted nitrogen fluence. The percentage of grains is determined from the statistics of the impact positions of the ions. As for samples with fluences of  $1 \times 10^{17}/\text{cm}^2$  and  $5 \times 10^{17}/\text{cm}^2$ , the calculated grain size is  $2.5 \times 10^{-11}\text{cm}^2$ . If the grain is assumed to be round, the grain length is 28 nm. This result fits very well with the experimental data shown in Fig. 3(c,d).

## Conclusions

An integrated technique that can be used for the preparation of  $\alpha'$ - $\text{Fe}_{16}\text{N}_2$  compound permanent magnets was proposed and demonstrated based on an ion implantation technology. In this approach, nitrogen ion implantation, direct bonding and a two-step annealing process were integrated for  $\text{Fe}_{16}\text{N}_2$  permanent magnet preparation. First, free-standing iron foil was bonded directly onto a silicon substrate. An ion implantation process was used to obtain an Fe-N mixture in iron foils. Different nitrogen implant fluences with the same implant energy were investigated. A pre-annealing step at  $500^\circ\text{C}$  for 0.5 hour was proposed and found to be crucial for three functions: (1) activating implanted nitrogen ions; (2) repairing the lattice damage; and (3) cleaning the sample surface. A post-annealing step at  $150^\circ\text{C}$  for 40 hours was found to assist nitrogen atom diffusion and form the chemically ordered  $\text{Fe}_{16}\text{N}_2$  phase in iron foils.

The M-H loop of a sample with  $5 \times 10^{17}/\text{cm}^2$  fluence showed explicit improvement of magnetic properties, especially showing magnetic hard behavior after the post-annealing step. To the best of our knowledge, this could be the first experimental evidence of the existence of a giant saturation magnetization, an obviously large

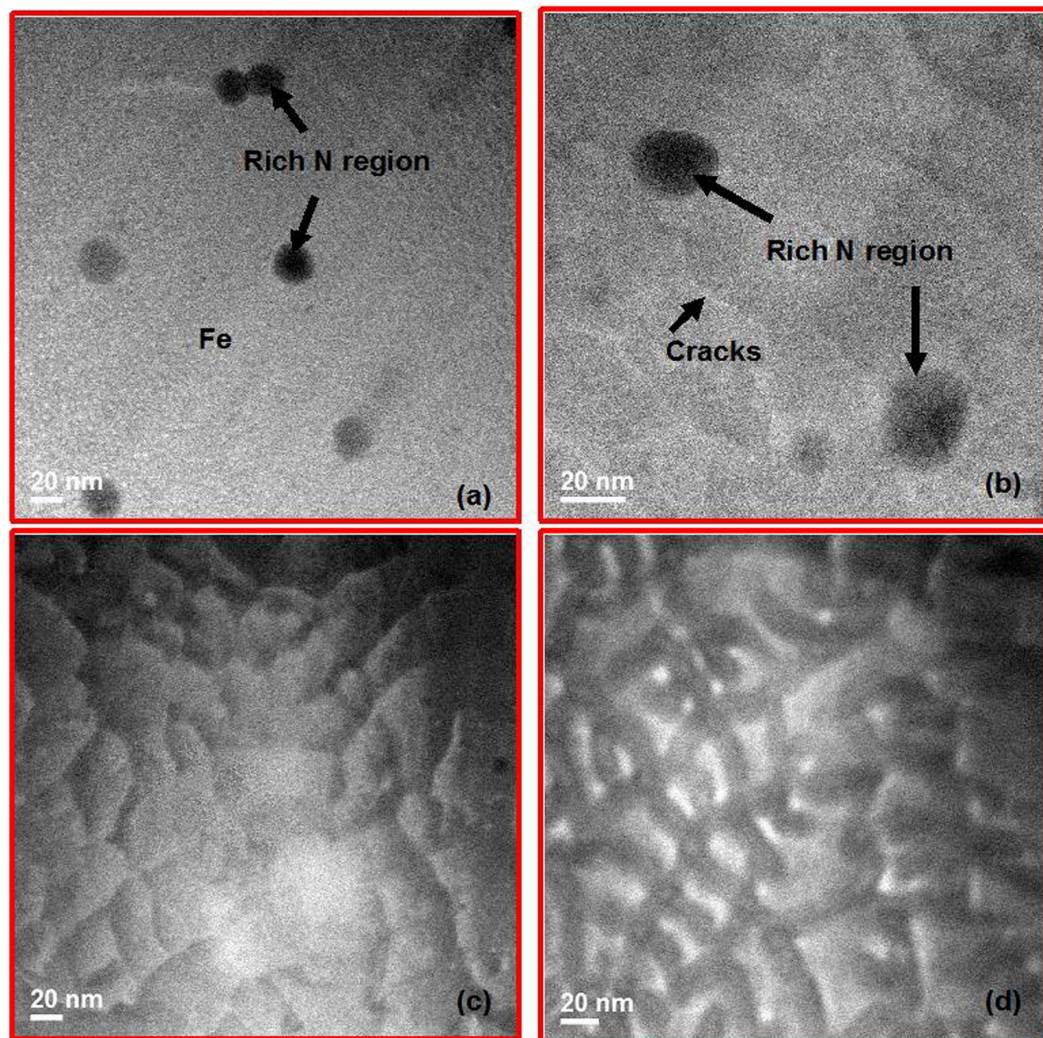


**Figure 3. Microstructures of the prepared samples, observed by high resolution transmission electron microscopy (HRTEM). (a)**  $2 \times 10^{16}/\text{cm}^2$  fluence, embedded dots can be observed (rich N region), with a diameter of 20 nm, separated by 140 to 200 nm; **(b)**  $8 \times 10^{16}/\text{cm}^2$  fluence, besides embedded dots, obvious cracks appeared; **(c)**  $1 \times 10^{17}/\text{cm}^2$  fluence, an obvious microstructure is generated, with diameter 20 to 40 nm; **(d)**  $5 \times 10^{17}/\text{cm}^2$  fluence, a microstructure with clear boundary is generated.

coercivity with a magnetic energy product of up to 20 MGOe in a bulk-type FeN sample. A granular structure was observed in the sample, in which a microstructure with 25–30 nm grains and obvious grain boundaries occurs.

**Experiment method.** Pure (110) iron foils with 500 nm thickness are positioned on mirror-polished (111) Si substrate. The surfaces of the substrates and iron foils are cleaned beforehand. The foils are directly bonded with the substrate using a wafer bonder in fusion mode (SB6, Karl Suss Wafer Bonder) at 450 °C for 30 minutes.

Nitrogen ion implantation was conducted at the Los Alamos National Laboratory. Ions of atomic  $\text{N}^+$  were accelerated to 100 keV and implanted into foils vertically with fluences ranging from  $2 \times 10^{16}/\text{cm}^2$  to  $1 \times 10^{18}/\text{cm}^2$  at room temperature. After that, a two-step post-annealing process was applied on the implanted foils. The first step was pre-annealing at 500 °C in  $\text{N}_2$  and Ar mixed atmosphere for 0.5 hour. Post-annealing followed at 150 °C for 40 hours in a vacuum.

## References

1. Chu, S. & Majumdar, A. Opportunities and challenges for a sustainable energy future. *Nature* **488**, 294–303 (2012).
2. Coey, J. M. D. Permanent magnet applications. *J. Magn. Magn. Mater.* **248**, 441–456 (2002).
3. Wang, J. P. *et al.* Fabrication of  $\text{Fe}_{16}\text{N}_2$  films by sputtering process and experimental investigation of origin of giant saturation magnetization in  $\text{Fe}_{16}\text{N}_2$ . *Magnetics, IEEE Transactions on* **48**, 1710–1717 (2012).
4. Ji, N. *et al.* Perpendicular magnetic anisotropy and high spin-polarization ratio in epitaxial Fe-N thin films. *Phys Rev B* **84**, 245310 (2011).
5. Sun, D. C., Jiang, E. Y., Tian, M. B., Lin, C. & Zhang, X. X. Epitaxial single crystal  $\text{Fe}_{16}\text{N}_2$  films grown by facing targets sputtering. *J. Appl. Phys.* **79**, 5440–5442 (1996).

6. Shinno, H. & Saito, K. Effects of film thickness on formation processes of Fe<sub>16</sub>N<sub>2</sub> in nitrogen ion-implanted Fe films. *Surf. Coat. Technol.* **103–104**, 129–134 (1998).
7. Nakajima, K. & Okamoto, S. Nitrogen-implantation-induced transformation of iron to crystalline Fe<sub>16</sub>N<sub>2</sub> in epitaxial iron films. *Appl. Phys. Lett.* **54**, 2536–2538 (1989).
8. Ogawa, T. *et al.* Challenge to the synthesis of  $\alpha''$ -Fe<sub>16</sub>N<sub>2</sub> compound nanoparticle with high saturation magnetization for rare earth free new permanent magnetic material. *Appl. Phys. Express* **6**, 073007 (2013).
9. Zulhijah, R. *et al.* Gas phase preparation of spherical core-shell  $\alpha''$ -Fe<sub>16</sub>N<sub>2</sub>/SiO<sub>2</sub> magnetic nanoparticles. *Nanoscale* **6**, 6487–6491 (2014).
10. Takagi, K. *et al.* High-pressure sintering behavior of  $\alpha''$ -Fe<sub>16</sub>N<sub>2</sub> nanopowder. *J. Appl. Phys.* **115**, 103905 (2014).
11. Jack, K. H. The occurrence and the crystal structure of  $\alpha''$ -iron nitride; a new type of interstitial alloy formed during the tempering of nitrogen-martensite. *Proc. R. Soc. London. A* **208**, 216–224 (1951).
12. Ji, N., Lauter, V., Zhang, X., Ambaye, H. & Wang, J. P. Strain induced giant magnetism in epitaxial Fe<sub>16</sub>N<sub>2</sub> thin film. *Appl. Phys. Lett.* **102**, 072411 (2013).
13. Herzer, G. Grain size dependent of coercivity and permeability in nanocrystalline ferromagnets. *Magnetics, IEEE Transactions on* **26**, 1397–1402 (1990).
14. Tong, W. P., Tao, N. R., Wang, Z. B., Lu, J. & Lu, K. Nitriding iron at lower temperatures. *Science* **299**, 686–688 (2003).
15. Ji, N., Liu, X. & Wang, J. P. Theory of giant saturation magnetization in  $\alpha''$ -Fe<sub>16</sub>N<sub>2</sub>; role of partial localization in ferromagnetism of 3d transition metals. *New J Phys* **12**, 063032 (2010).
16. Iverson, R. B. & Reif, R. Stochastic model for grain size versus dose in implanted and annealed polycrystalline silicon films on SiO<sub>2</sub>. *J. Appl. Phys.* **57**, 5169–5175 (1985).
17. Nakajima, K. & Okamoto, S. Nitrogen-implantation-induced transformation of iron to crystalline Fe<sub>16</sub>N<sub>2</sub> in epitaxial iron films. *Appl. Phys. Letter* **54**, 2536–2538 (1989).
18. Zeng, H., Li, J., Liu, J. P., Wang, Z. L. & Sun, S. Exchange-coupled nanocomposite magnets by nanoparticle self-assembly. *Nature* **420**, 395–398 (2002).
19. Weber, T., De Wit, L., Saris, F. W. & Schaaf, P. Search for giant magnetic moments in ion-beam-synthesized  $\alpha''$ -Fe<sub>16</sub>N<sub>2</sub>. *Thin Solid Films* **279**, 216–220 (1996).
20. Kikkawa, S. *et al.* Formation of iron nitrides applying N<sup>+</sup> ion implantation. *Vacuum* **47**, 863–866 (1996).
21. Jagielski, J., Kopcewicz, M., Gawlik, G., Matz, W. & Thome, L. Thickness dependent phase transformations in implanted iron layers. *J. Appl. Phys.* **91**, 6465–6470 (2002).
22. Yamanaka, K. *et al.* Humidity effects in Fe<sub>16</sub>N<sub>2</sub> fine powder preparation by low-temperature nitridation. *J. Solid State Chem.* **183**, 2236–2241 (2010).
23. Yamashita, K. *et al.* Crystal structure and magnetic property of " $\alpha''$ -Fe<sub>16</sub>N<sub>2</sub>" containing residual  $\alpha$ -Fe prepared by low temperature ammonia nitridation. *J. Solid State Chem.* **194**, 76–79 (2012).
24. Jiang, Y. F., Zhang, X., Mehedi, A. A., Yang, M. & Wang, J. P. A method to evaluate  $\alpha''$ -Fe<sub>16</sub>N<sub>2</sub> volume ratio in FeN bulk material by XPS. *Materials Research Express* **2**, 116103 (2015).
25. Jaccodine, R. J. Surface energy of Germanium and Silicon. *J. Electrochem. Soc.* **110**, 524–527 (1963).
26. Schönecker, S., Li, X., Johansson, B., Kwon, S. K. & Vitos, L. Thermal surface free energy and stress of iron. *Sci. Rep.* **5**, 14860 (2015).
27. Arnott, R. J. & Wold, A. The preparation and crystallography of FeNiN and The series Fe<sub>4-x</sub>Ni<sub>x</sub>N. *J. Phys. Chem. Solids* **15**, 152–156 (1960).
28. Liu, J. P., Luo, C. P., Liu, Y. & Sellmyer, D. J. High energy products in rapidly annealed nanoscale Fe/Pt multilayers. *Appl. Phys. Lett.* **72**, 483–485 (1998).
29. Tessier, F. *et al.* Energetics of binary iron nitrides. *Solid State Sciences* **2**, 457–462 (2000).
30. Inia, D. K., Pröpper, M. H., Arnoldbik, W. M., Vredenberg, A. M. & Boerma, D. O. Low-temperature nitriding of iron through a thin nickel layer. *Appl. Phys. Lett.* **70**, 1245 (1997).
31. Arsenault, R. J. & Shi, N. Dislocation generation due to differences between the coefficients of thermal expansion. *Mater. Sci. Eng.* **81**, 175–187 (1986).

## Acknowledgements

This work was supported in part by ARPA-E (Advanced Research Projects Agency-Energy) BCT Fe<sub>16</sub>N<sub>2</sub> Magnet project under contract No. 0472–1595. Parts of this work were carried out in using the Characterization Facility, which receives partial support from NSF through the NSF Minnesota MRSEC program under Award Number DMR-0819885. Ion implantation was supported by Center for Integrated Nanotechnologies (CINT), a DOE nanoscience user facility jointly operated by Los Alamos and Sandia National Laboratories.

## Author Contributions

J.-P.W. conceived the experiments and coordinated the research. Y.J. and M.A.M. prepared and characterized the samples; E.F. and Y.W. conducted ion implantation experiments; L.F.A. took HRTEM and diffraction images. Y.J. and J.-P.W. analyzed the data and wrote the manuscript with the contribution from other authors.

## Additional Information

**Supplementary information** accompanies this paper at <http://www.nature.com/srep>

**Competing financial interests:** Dr. Jian-Ping Wang has equity and royalty interests in, and serves on the Board of Directors and the Scientific Advisory Board, for Niron Magnetics LLC, a company involved in the commercialization of FeN magnet. The University of Minnesota also has equity and royalty interests in Niron Magnetics LLC. These interests have been reviewed and managed by the University of Minnesota in accordance with its Conflict of Interest policies. All other authors declare no competing financial interests.

**How to cite this article:** Jiang, Y. *et al.* Synthesis of Fe<sub>16</sub>N<sub>2</sub> compound Free-Standing Foils with 20 MGOe Magnetic Energy Product by Nitrogen Ion-Implantation. *Sci. Rep.* **6**, 25436; doi: 10.1038/srep25436 (2016).



This work is licensed under a Creative Commons Attribution 4.0 International License. The images or other third party material in this article are included in the article's Creative Commons license, unless indicated otherwise in the credit line; if the material is not included under the Creative Commons license, users will need to obtain permission from the license holder to reproduce the material. To view a copy of this license, visit <http://creativecommons.org/licenses/by/4.0/>